MedRes: a new MEDium RESolution integral field spectrograph for SPHERE

Raffaele Gratton[a], Cristoph Keller[b,c], Emiliano Diolaiti[d], Andrea Baruffolo[a], Mickael Bonnefoy[e], Valentina D'Orazi[a], Maud Langlois[f], Magali Loupias[f], Mamadou N'Diaye[g], Eric Pantin[h], Eric Stadler[e], François Wildi[i], Jean-Luc Beuzit[j], Anthony Boccaletti[k], Gael Chauvin[g], Silvano Desidera[a], David Mouillet[e], Andrea Bianco[l], Enrico Cascone[m], Fausto Cortecchia[d], Vincenzo De Caprio[m], Adriano De Rosa[d], Celia Desgrange[e], Michele Frangiamore[l], Rico Landman[b], Matteo Lombini[d], Giuseppe Malaguti[d], Dino Mesa[a], Julien Milli[e], Gianluca Morgante[d], Thibault Pichon[h], Filomena Schiavone[d], Laura Schreiber[d], Luca Terenzi[d], and Alessio Zanutta[l]

[a]INAF Osservatorio Astronomico di Padova, Vicolo dell'Osservatorio 5, 35122, Padova, Italy
[b]Leiden Observatory, Leiden University, PO Box 9513, 2300 RA Leiden, The Netherlands
[c]Lowell Observatory, 1400 W Mars Hill Rd, Flagstaff, AZ 86001, Arizona, USA
[d]INAF Osservatorio di Astrofisica e Scienza dello Spazio di Bologna, Via P. Gobetti 93/3, 49129, Bologna, Italy
[e]Univ. Grenoble Alpes, CNRS, IPAG, 38000 Grenoble, France
[f]Univ Lyon, Univ Lyon1, Ens de Lyon, CNRS, Centre de Recherche Astrophysique de Lyon UMR5574, F-69230, Saint-Genis-Laval, France
[g]Université Côte d'Azur, Observatoire de la Côte d'Azur, CNRS, Laboratoire Lagrange, France
[h]AIM, CEA, CNRS, Université Paris-Saclay, Université Paris Diderot, France
[i]Geneva Observatory, University of Geneva, Geneva, Switzerland
[j]Aix Marseille Universit, CNRS, LAM, UMR 7326, 13388, Marseille, France
[k]LESIA, Observatoire de Paris, PSL Research Univ. CNRS, Meudon, France
[l]INAF Osservatorio Astronomico di Brera, Via Brera 28, 20121, Milano, Italy
[m]INAF Osservatorio Astronomico di Capodimonte, Salita Moiariello 16, 80131 Napoli, Italy

ABSTRACT

MedRes is a proposed MEDium RESolution integral field spectrograph for upgrading SPHERE, the high contrast instrument for the ESO VLT telescope. MedRes is actually thought of as a potential Visitor Instrument with the scope to provide high contrast diffraction limited medium-high resolution spectra ($R \geq 1000$) over a reasonably large field of view (a square with a side of at least 0.4) and across the spectral region 1.2-1.65 microns. Two main science objectives are driving the proposition for such an instrument on SPHERE. First of all, MedRes shall improve the detection of previously unknown giant planets (contrast 10^{-5}, goal 10^{-6}), in particular accreting planets, at small separation from the star (< 0.2", goal, 0.1"). And second, MedRes will boost the characterisation of known (faint) planets at a spectral resolution substantially higher than currently possible with SPHERE IFS ($R \sim 35 - 50$) and for contrasts much better than achievable with IRDIS Long Slit Spectroscopy (LSS) at small separations. The design will be optimised for SPHERE, fully exploiting the capabilities offered by a second stage Adaptive Optics (SAXO+) and complementing the niches of IRDIS, IFS and HiRise in the near IR channel. A preliminary optomechanical design and simulations of performance will be presented.

Keywords: Spectrographs, High Contrast Imaging, Integral Field Units, Optical Fibers, VPH, VLT

Further author information: (Send correspondence to R.G.)
R.G: E-mail: raffaele.gratton@inaf.it, Telephone: +39 049 8293442

1. INTRODUCTION

The Spectro-Polarimetric High-contrast Exoplanet REsearch instrument (SPHERE[1]) has now been in operation at the VLT for more than seven years, demonstrating a high level of performance. SPHERE has produced outstanding results using a variety of operating modes, primarily in the field of direct imaging of exoplanetary systems, focusing on exoplanets as point sources and circumstellar disks as extended objects with about 300 refereed publications. This motivated a large consortium to propose an even more ambitious set of science cases, and its corresponding technical implementation in the form of an upgrade. The SPHERE+[2] project capitalises on the expertise and lessons learned from SPHERE to push high contrast imaging performance to its limits on the VLT 8m-telescope.

1.1 Scientific goals

The main motivation for SPHERE+ relies on three key scientific requirements that are currently driving this project as well as our proposed instrumental concept.

- **sci.req.1** - Access the bulk of the young giant planet population down to the snow line (3-10 au), in order to bridge the gap with complementary techniques (radial velocity, astrometry), taking advantage of the synergy with Gaia, and to explore for the first time the complete demographics of young giant planets at all separations in order to constrain their formation and evolution mechanisms.
- **sci.req.2** - Observe a large number of fainter (lower mass) stars in the youngest (1-10 Myr) associations (Lupus, Taurus, Chamaeleon, Scorpius-Centaurus...), to directly study the formation of giant planets in their birth environment, building on the synergy with ALMA to characterise the architectures and properties of young protoplanetary disks, and how they relate to the population of planets observed around more evolved stars.
- **sci.req.3** - Improve the level of characterisation of exoplanetary atmospheres by increasing the spectral resolution in order to break degeneracies in giant planet atmosphere models and to measure abundances and other physical parameters, such as the radial and rotational velocities. Near-infrared will be the primary wavelength range utilised, but the visible range also delivers valuable information in the form of accretion tracers.

The SPHERE+ top level requirements connected to the proposed science cases can be summarised by going closer, deeper, and fainter. As we understand very well the limitations of SPHERE, the science requirements can be linked directly to the following instrumental requirements:

- **tech.req.1** - Deeper/closer: increase the bandwidth of the xAO system (typically 3kHz instead of 1kHz) and improve the correction of non-common path aberrations and coronagraphic rejection.
- **tech.req.2** - Fainter: include a more sensitive wavefront sensor to gain 2-3 magnitudes for red stars.
- **tech.req.3** - Enhanced characterisation: develop spectroscopic facilities with significantly higher spectral resolution compared to the current SPHERE Integral Field Spectrograph (IFS[3]). In this respect, both medium ($R \sim 1000$) and high ($R \sim 50000$) resolutions are extremely valuable for the characterisation of planetary atmospheres.

Besides better characterisation, a higher spectral resolution than the current SPHERE IFS allows application of alternative techniques for high contrast imaging. In fact, the SPHERE IFS was optimised for removal of speckle noise through application of Angular Differential Imaging (ADI[4]) and Spectral Differential Imaging (SDI[5]). However, even when combined,[6] these techniques are not very efficient at very short separation from the star because both depends on the separation in units of λ/D. An appealing technique in this case may be molecular mapping,[7] whose applicability is independent of separation - though of course is advantaged by a lower background noise. The spectral resolution offered by the current IFS is clearly not adequate for molecular mapping; this calls for a medium resolution spectrograph that fully exploits the very high contrast at low separations provided by SPHERE+.

1.2 MedRes in the SPHERE+ context

Following these technical specifications, SPHERE+ mainly consists of two modules: (i) SAXO+,[8,9] a second stage of AO providing a fast (ideally up to 3 kHz) correction of low order aberrations, to improve contrast at very small separation from the star (down to the coronagraphic edge); and (ii) MedRes, a new MEDium RESolution ($R \sim 1000$) integral field spectrograph for SPHERE. MedRes is actually conceived as a potential Visitor Instrument for VLT and a demonstrator for the use of very low noise detectors on high contrast imaging instruments. The high resolution ($R \sim 50000$) spectroscopic mode is the scope of a separate project, HiRISE.[10]

MedRes is quite independent of SAXO+: it optimises the performances offered by SAXO+, but it is a very valuable instrument by itself when coupled with current SPHERE. However, MedRes and SAXO+ are developed as a unique project (SPHERE+) by the same Consortium and with the same science goal (better understanding the formation of giant planets).

2. DETERMINATION OF TOP LEVEL REQUIREMENTS

The scope of MedRes is to provide high contrast diffraction limited medium-high resolution spectra ($R > 1000$) over a reasonably large space area (a square with a side of at least 0.4 arcsec) over the spectral region 1.2-1.65 micron for: (i) Detection of previously unknown faint sources (contrast up to 10^{-5}, ideally 10^{-6}), in particular accreting planets, at small separation from the star (< 0.2 arcsec, ideally performances should be verified down to 0.1 arcsec); (ii) characterisation of known (faint) planets at a resolution substantially higher than possible with SPHERE IFS (that offers up to $R \sim 50$) and for contrasts much better than possible with IRDIS LSS. A typical benchmark is PDS-70b, the goal being detection of the H-emission lines with $SNR > 10$ and the continuum spectrum with $SNR > 5$.

The design will be optimised for SPHERE, fully exploiting the capabilities offered by SAXO+ and complementing the niches of IRDIS, IFS and HiRise in the NIR channel, but other feeds including SCExAO and MagAO-X will be possible.

2.1 Noise model and parameter optimization

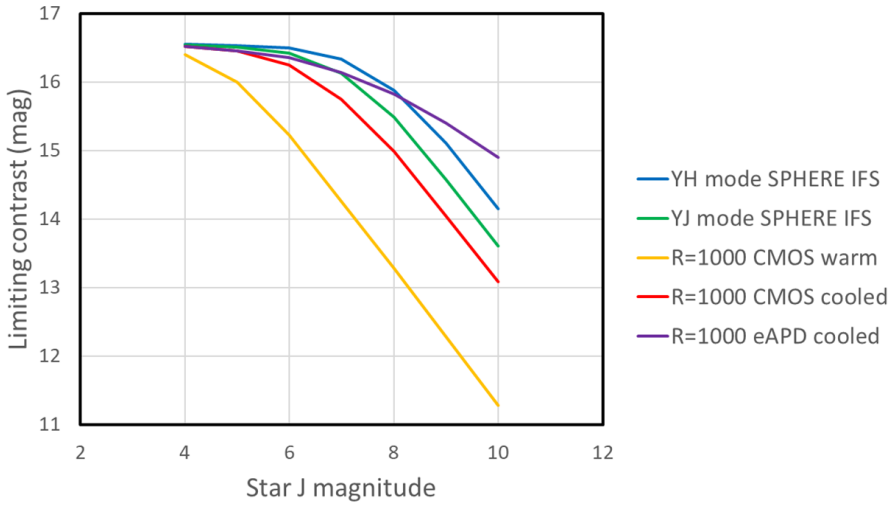

Figure 1. Run of the limiting contrast at 0.2 arcsec as a function of stellar magnitude in typical observing conditions at VLT for the SPHERE Integral Field Spectrograph IFS and for alternative schemes of medium resolution integral field spectrographs.

We prepared a zero order noise model in order to explore the relevance of the main design choice. The result of this model is the limiting contrast as a function of the magnitude of the star (see Fig.1). The model considers various sources of noise: the noise due to the star background (both photon noise and the residual speckle noise

after application of differential imaging), the faint companion photon noise, and the noise due to the detector and to the thermal background of the instrument. This model has been calibrated in order to reproduce the observations gathered over seven years with the IFS. We assumed a spectral resolution of $R = 1000$ for MedRes, and various alternative designs. We found that if MedRes is at room temperature - as it is the case of IFS - the thermal background from the instrument is the dominant source of noise for all but the brightest targets*. We will then assume that MedRes is cooled - a temperature of -50 C is enough to make the thermal background negligible with respect to other sources of noise. If MedRes is cooled, then the major source of noise for most cases is the detector. It is then very important that the noise associated to the detector is as as low as possible. We will then analyse the possibility of replacing CMOS detectors, such as the Hawaii II detector used for the SPHERE IFS that have read out noise (RON) of the order of a few electrons, with electron Avalanche Photodiode Arrays (eAPD[11]) that may have an order of magnitude lower level of noise. This point will be discussed a bit more in detail in Section 3.3.

2.2 Parameter optimisation

Following this first exploration, MedRes is made of two main modules:

- An integral field unit (IFU) either based on lenslets or on fibers or both
- A cooled spectrograph designed around a medium/large format eAPD detector

The spectrograph is small (but its size scales with the field of view of the IFS) due to the diffraction-limited input and can be largely based on existing designs. The choice of spectral resolution will require a careful analysis using end-to-end simulations that include the data analysis, and different detector options will have to be analysed. The IFU itself will also require a careful trade-off study. In fact, while a lenslet based design offers a higher efficiency and a larger number of spaxels, the fiber design is more flexible and allows some improvement in the contrast due to the filtering of speckles provided by single mode fibers.[12,13] Mitigation of the low efficiency of fibers can be obtained by using three-dimensional printed lenses on top of a single-mode multicore fiber.[12]

The design of MedRes should be done considering error budget at a system level. The trade-off study should consider the compromises between: (i) number of spaxels and number of spectral elements (limited by detector size); (ii) field of view and resolution on sky (limited by the number of spaxels); (iii) spectral resolution and spectral coverage (limited by the number of spectral elements); (iv) efficiency and possible implementation on SPHERE; (v) detector size and RON characteristics that limit performances on faint targets. This should be done through noise budget evaluation and end-to-end simulations.

2.3 Summary of parameters

Figure 2 summarises the main parameters for the two schemes that consider an IFU made of optical fibers and of a lenslet array, respectively. In particular, the efficiency considered for the lenslet array design is based on the experience gathered with the SPHERE IFS,[1] while that for the fiber design uses data from Haffert et al.[12]

3. SKETCH OF A PRELIMINARY DESIGN

We prepared a preliminary design for MedRes that exploits a $1k \times 1k$ eAPD detector (see Fig. 3). This scheme assumes a lenslet based IFU similar to that considered for the current SPHERE IFS[3] that uses a BIGRE scheme.[14] The lenslet array feeds an afocal spectrograph. Two separate dewars are considered: the first collimator and the last camera lenses are the entrance and exit window of the spectrograph dewar that is cooled at a moderately low temperature; the last camera lens is the entrance window of the detector dewar that is cooled at LN2 temperature. This spectrograph has a resolution of $R = 1000$ and may observe alternatively the J and H-band with two different dispersers, mounted on a (cool) slide. A second feeding by fibers providing a higher resolution

*The SPHERE IFS was designed for observing targets down to magnitude $J = 8$ at $R = 50$. because of the lower spectral resolution of that spectrograph, thermal and detector noise are not the dominant source of noise at this magnitude. Cooling only the detector simplified instrument design and make it much more reliable. However, increasing spectral resolution dilutes photons from the target over a wider detector area modifying this case.

Concept	Specification	Goal
Fiber-fed		
spaxel sampling	1 l/D (32 mas (J))	1 l/D (32mas (J))
FoV (diameter)	11x11 (352 mas)	15 x 15 (480 mas)
transmission/efficiency	30%	50%
resolution	5000	5000
spectral range	J or H simult.?	J or H simult. ?
Nb spectral elements	2 x 1K	2 x 1K
Detector: size	512x512	1K x 1K
Detector: T, RON	220K, 1.0	220K, 0.2
Cooling	yes	yes
Lenslet		
spaxel sampling	0.5 l/D (16 mas J)	0.5 l/D (16 mas J)
FoV (diameter)	35x35 (560 mas) 47x47 (720 mas)	35x35 (560 mas) 47x47 (720 mas)
transmission/efficiency	60%	60%
resolution	1000	1000
spectral range	J or H (not simult.), 1/10 bandwidth	J or H (not simult.), 1/10 bandwidth
Nb spectral elements	200 (R=1000) 100 (R=500)	200 (R=1000) 100 (R=500)
Detector: size	512x512	1K x 1K
Detector: T, RON	220K, 1.0	220K, 0.2
Cooling	yes	yes

Figure 2. Main specifications for MedRes

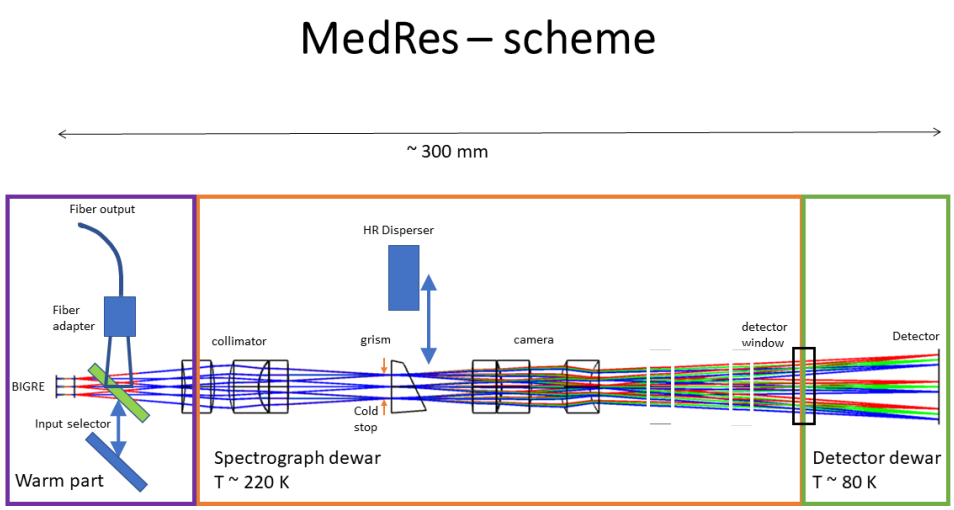

Figure 3. Schematic design of MedRes

of $R = 5000$ is possible by inserting a removable (warm) 45 degrees mirror just in front of the collimator and having a third disperser on the (cool) slide. A suitable optics interface should be inserted between the fiber exit and the spectrograph. In addition, a suitable optical interface should allow feeding MedRes within SPHERE (or alternative high contrast imagers).

3.1 First-order paraxial design

We used the same spreadsheet prepared for the SPHERE IFS to obtain the paraxial parameters for MedRes. This software uses the equations describing a BIGRE based spectrograph[14] and allows for a fast exploration of

possible parameter designs, providing approximate values for the most important parameters, including a first guess for the size of the instrument that is a crucial parameter since MedRes should fit within SPHERE.

The preliminary solution considers a 35 × 35 hexagonal lenslet BIGRE IFU device (diameter 6 mm) that represents the optical interface of MedRes with modified SPHERE+ Common Path optics (CP). The BIGRE is located on a re-imaged telescope focal plane and needs to be fed with an input focal ratio equal to F_{tel}= 201.6. This request satisfies the Shannon's sampling criterion of the re-imaged post-coronagraphic speckles pattern ($\lambda/D = 0.5$) at the shortest wavelength (1.20 μm) for the adopted pitch of the BIGRE lenslet array (130 μm). The field of view is roughly square with a side of 0.57 arcsec, exploiting the area where SAXO+ offers the largest advantage with respect SAXO alone. The BIGRE array has a demagnification factor of K=8.2 in order to provide enough room for the spectra. The spectrograph magnification is of 3.45 in order to provide the correct (super)sampling of the spectrum on the detector - that have pixels of 15 μm. Using the same notation used for the SPHERE IFS, we adopted an hexagonal-F configuration, where the dispersion direction is rotated by 52.4 degree with respect the line connecting the lenslet centres. In this configuration, spectra (aligned along detector columns) may have a length of 193 pixels allowing to obtain $\lambda/10$ spectral coverage at a resolution of $R \sim 1000$. The spectra are separated by 4.27 pixels in the direction perpendicular to dispersion, allowing appropriate determination of the local background when extracting the spectra.

3.2 MedRes optical design and quality description

MedRes is a BIGRE-oriented IFS instrument for SPHERE+, adopting standard dioptric devices.[14] An additional fibre mode configuration is under study; in this case, MedRes will be fed by optical fibre by means of a folding mirror inserted between BIGRE and the first collimator lens. The main features of the designs of the MedRes are summarised in Fig. 4; in the current section, we briefly describe the MedRes optical design.

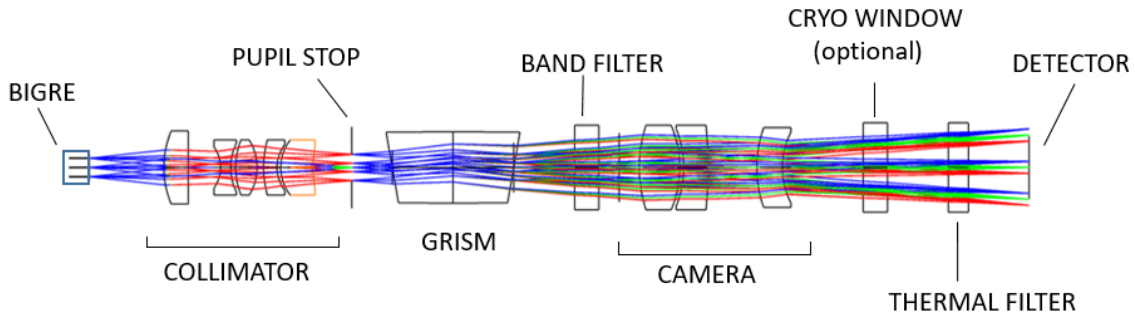

Figure 4. MedRes sub-systems.

The input optical beam should be telecentric in order to guarantee that the condition of Fraunhofer's optical propagation holds between all the conjugate optical planes of MedRes. The MedRes optics is composed by 6 main sub-systems (Fig. 4): BIGRE IFU, collimator optics, pupil stop, disperser optics, camera optics, filters and cryostat optics. The instrumental background radiation is controlled by cooling down MedRes to -50 C, imposing a considerable distance between the aperture in the cryogenic shield and the detector and using a suitable chromatic low pass filter cutting wavelengths. The collimator's first lens behaves as MedRes window and delimits the cold area of MedRes; only the first collimator lens and the BIGRE IFU share the same environmental temperature as the common path.

Fig. 5 shows the MedRes ray-tracing without filters, grism and cryogenic window, and Fig. 6 shows the spot quality of MedRes collimator/camera (i.e. without BIGRE, filters, grism and cryogenic window).

OHARA glasses have been selected (equivalent glasses from other manufacturers can be used): S-FPL51, S-FPM2, S-LAL20, S-LAH89, S-NBH5, S-TIH11, and S-TIH53. In addition to these glasses, IR-grade Fused Silica has also been used in the design.

A preliminary analysis of MedRes dispersers has also been performed. In BIGRE configuration, two operation modes with $R = 1000$ are foreseen (Fig. 2): the first covers the J band (1.20 ÷ 1.33 micron), and the second

covers the H band (1.56 ÷ 1.72 micron). Tab. 1 shows the $R1000$ grisms characteristics. One more disperser with $R = 5000$ is under evaluation and shall be used in the MedRes fibre-fed configuration. All dispersers will be mounted on a linear stage, or a wheel, close to the cold pupil stop.

Grooves (l/mm)	Diffr.Order	Half-angle (°)	Glass	Configuration	Resolution
208.0	1	10.0	S-TIH11	BIGRE - J (1.20 ÷ 1.33 micron)	1000
159.8	1	10.1	S-TIH11	BIGRE - H (1.56 ÷ 1.72 micron)	1000

Table 1. MedRes preliminary grism units characteristics.

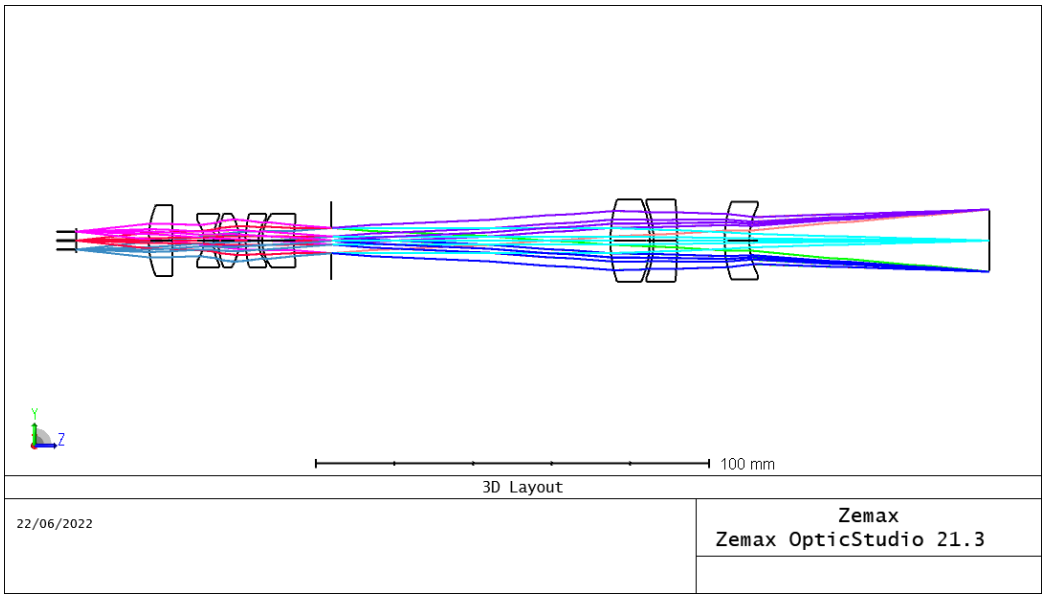

Figure 5. Ray-tracing of the assembled MedRes (i.e. BIGRE, collimator and camera). Object space focal ratio is $F_{in} = 40.28$. Image-space focal ratio is $F_{cam} = 16.95$. The imaged field of view on sky is a 0.77 arc-seconds diagonal.

3.3 Detector

As mentioned in Sect. 2, in the current design where MedRes is cooled, the major source of noise for most science cases is the detector. There is then a large gain replacing CMOS detectors, such as the Hawaii II detector used for the SPHERE IFS that have read out noise (RON) of the order of a few electrons, with electron Avalanche Photodiode Arrays (eAPD[11]) that may have an order of magnitude lower level of noise. eAPD detectors are now available in medium-to-large formats, up to 1k×1k and even 2k×2k in the near future.

While the format of currently available eAPD detectors is smaller than possible with CMOS detectors, their size is possibly enough for the purposes of MedRes; in fact, as mentioned before, one of the main parameter choice for MedRes is the need to fit within the room available on SPHERE, and this is much easier if the spectrograph is very compact, a condition that it is easier to realise for a small field integral field unit. MedRes may be among the first astronomical instruments exploiting a moderately large format eAPD detector for science purpose; it may then be considered as a prototype for their application on future instruments on extremely large telescopes.

During the preliminary study phase of MedRes, it will be assessed, based on already published results, if an eAPD detector would fulfil the detectors requirements and specifications. The performances of an eAPD will also be compared against that of the well-known/well-characterised Teledyne Hawaii II-RG detector. A trade-off study will be conducted in terms of detectors performances and specifications compliance, detector costs, availability of turnkey packaging (mechanical, electrical, and cryogenic) solutions, need for a complete characterisation, and the availability of the detectors in the procurement phase. Indeed, the development of a detector socket, setting-up the electrical, mechanical, and thermal interfaces, the development or the adaptation of a detector controller,

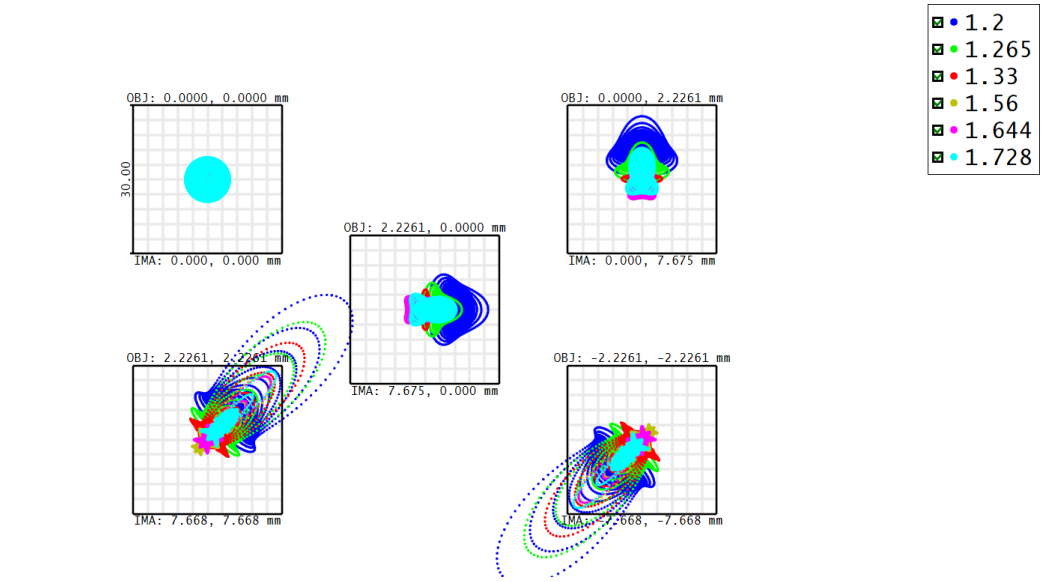

Surface IMA: CAM FP

Spot Diagram	
22/06/2022 Units are µm. Legend items refer to Wavelengths	Zemax Zemax OpticStudio 21.1

Field	1	2	3	4	5
RMS radius	3.012	3.611	3.611	5.539	5.539
GEO radius	4.520	12.807	12.807	39.436	39.436

Box width : 30 Reference : Chief Ray

Figure 6. Collimator/camera spot diagrams, from the on-axis to the extreme off-axis fields ± 3.148 mm. Different colours are for different wavelengths; the detector pixel size is 15 micron, and the box is 30 micron.

and a complete detector characterisation, require a consequent amount of human resources and the availability of testbeds that must be taken into account. The trade-off study aims at evaluating the costs, both in terms of cash and human resources, of the different solutions, so that the best compromise can be identified.

3.4 Cryogenic scheme

The thermal architecture is under study at the moment of this writing. A possible solution is a single vacuum volume shared by two cold assemblies (Fig. 7):

- optics, barrels and translation stage cooled at 220K by a thermal electric cooler element (the vessel containing these parts is highlighted in green in Fig. 7);
- detector, baffle and filters cooled at 80K by a closed cycle cooler (these parts and the cryostat enclosing them are highlighted in blue in Fig. 7).

This choice leads to a compact design that fulfils the volume constraints to fit MedRes into the SPHERE's existing enclosure. In order to limit the radiative transfers to the cold optics (enclosed in the barrels depicted in red), both the inner surfaces of the vessel and the external surfaces of the barrels have to be polished. On the other hand, the inner surfaces of the barrels need to be coated with an infrared absorbing treatment. The thermal electric cooler used for cooling down the optical path is cooled down itself by sharing the water cooling circuit with the closed cycle cooler for the detector. For the grisms exchanging system, two possible solutions are considered at the moment. The first one is based on a piezoelectric miniature translation stage compatible with vacuum and cold environment, and the second solution is a simple translation stage where a standard motor is placed outside the vessel with a mechanical feed through. The collimator's first lens closes the vacuum vessel.

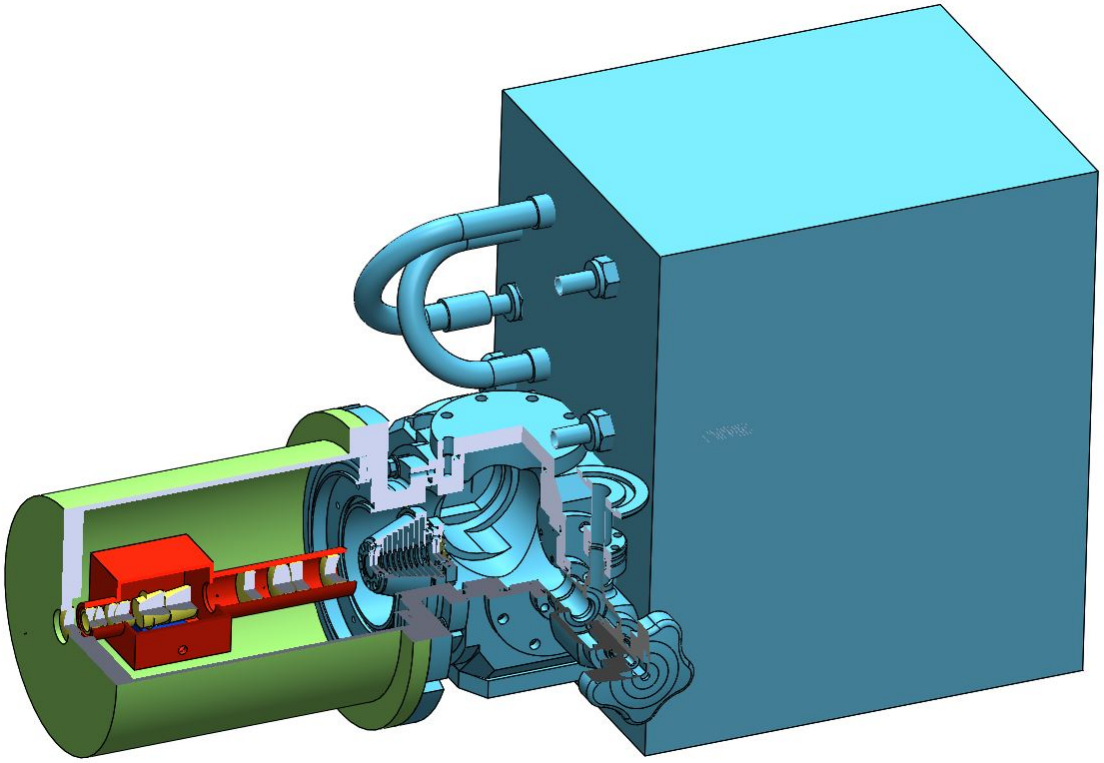

Figure 7. MedRes cryogenic scheme: the vessel containing the optics is highlighted in green; the optics barrels are highlighted in red; the camera is coloured blue.

3.5 Implementation within SPHERE

MedRes is fed by the AO-corrected optical beam of SPHERE through a dedicated channel. The optical beam, which runs parallel to the main optical bench, is picked-off by a deployable flat mirror and folded upwards; two lenses adapt the focal ratio, as required by the spectrograph, and the pupil position (nominally at infinity); finally, a second flat mirror folds the optical beam and sets it parallel again to the main optical bench, placing the entrance focal plane for MedRes at the required position within the SPHERE volume. The spectrograph optical axis is about 400 mm above the main optical axis: this choice is imposed by space limitations. Several options for the position of MedRes within the SPHERE instrument volume are under investigation and traded-off, taking into account several aspects, such as accessibility, availability of fixation points on the main bench, thermal effects, compactness of optical path and thus stability. The current working baseline is shown in Fig. 8: the position of MedRes is close to the SPHERE's optical bench centre of gravity. Incidentally, the assembly consisting of the green structure and blue camera to the left of MedRes in the same figure is the opto-mechanical module of SAXO+.

4. SIMULATIONS

We perform numerical simulations of SPHERE with the MedRes module to estimate the achievable contrast with a new medium resolution mode, perform some trade-off analysis with different instrument characteristics (e.g. spectral resolution, bandwidth, field of view) for an optimal science return, and further explore novel scientific cases with this new facility.

4.1 Simulation framework

For a given star-planet system, MedRes will provide IFS data cubes on which different post-processing methods can be applied to retrieve and spectrally analyse the planetary signal. In our preliminary work, we do not

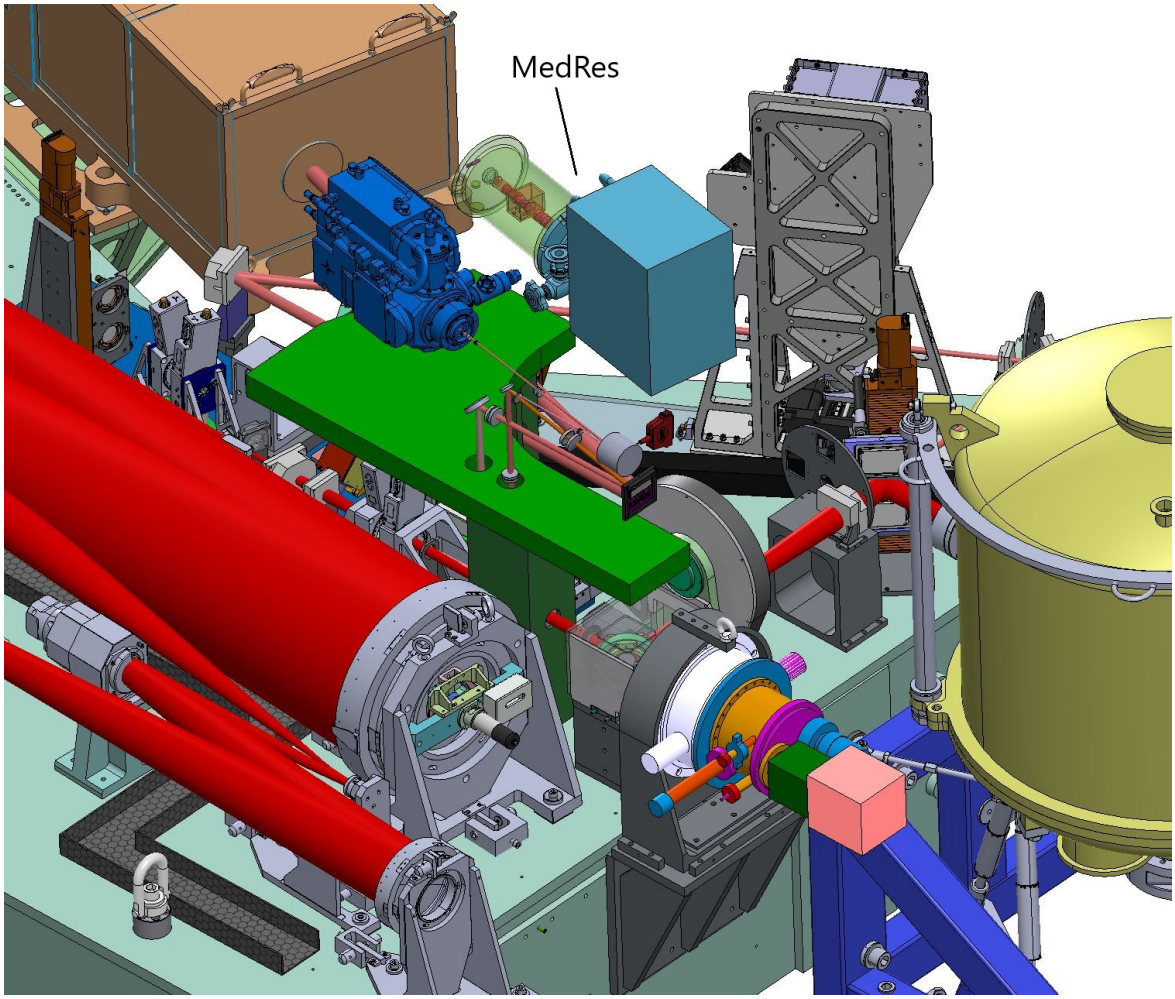

Figure 8. Possible implementation of MedRes within the SPHERE instrument.

consider extensive temporal evolution. Temporal field rotation and the possible contrast improvement provided by Angular Differential Imaging (ADI[4]) are therefore left for further studies. In the current framework, we only investigate the contrast gain related to Spectral Differential Imaging (SDI) using the molecular mapping reduction technique.[7]

4.1.1 Generation of spectral cubes using AO residuals and coronagraphy

Based on the Fourier-based formalism, we model the SPHERE+MedRes combination to produce simulated data cubes. Our framework relies on the simulation work that was established for the on-sky validation of the ZELDA sensor in SPHERE, see the appendix B of the corresponding paper.[15]

To simulate the AO residuals from the SPHERE extreme adaptive optics (ExAO) SAXO,[16] we have the 41,400 available wavefront errors maps from the 30 s real-time on-sky telemetry data with a 1380 Hz AO loop speed that were obtained during the ZELDA sensor tests in April 2018.[15] For this data set, the observing conditions were typical with a bright star, a seeing of 0.7", and a coherence time of 5 ms. These AO residual wavefront error maps correspond to a combination of reconstructed tip and tilt, reconstructed high-order modes, and simulated aliasing and fitting errors. As shown in the context of ZELDA on-sky experiments,[15] the simulated images with the reconstructed ExAO phase screens are in good agreement with the acquired data, therefore making these ExAO screens a good representing data set for the generation of our MedRes data cubes with SAXO.

As only 30 s of AO wavefront maps is available, we artificially modify this duration to produce IFS data cubes

with integration time from a few seconds to minutes. In further studies, we will generate new AO residuals maps by relying on the power spectral density of the currently data set to increase the number of realizations to produce cubes with larger integration time. Several additional limitations such as quasi-static errors, static errors, low-wind effects, wind-driven halo, chromatic errors are also known to possibly mitigate the image contrast.[17] In our preliminary simulations, we limit the number of the known effects for the sake of simplicity and additional effects will be considered in the near future. Finally, while our current study is limited to SAXO, further simulations will include SAXO+ characteristics to estimate its impact on the science return with MedRes.

Our simulations also include the SPHERE apodized pupil Lyot coronagraph[18,19] with the apodizer APO1, the 92.5 mas radius opaque focal plane mask ALC2 and the Lyot stop STOP_ALC2[1] for star diffracted light suppression. Manufacturing and wavefront errors from the coronagraph parts are also taken into account in the simulations and further details can be found in the ZELDA on-sky validation paper.[15]

Based on this SPHERE AO and coronagraph framework, several cubes are generated in J- or H-bands using the central wavelength λ_c and the width $\Delta\lambda$ of the spectral band for the corresponding BB_J (λ_c=1245 nm and $\Delta\lambda$=240 nm) and BB_H broadband filters (λ_c=1625 nm and $\Delta\lambda$=290 nm). Narrow band filters can also considered to explore bandwidth trade-off studies. For the spectral cube characteristics, we assume Nyquist spectral sampling and a spectral resolution with a regular spectral sampling as a zero-order implementation. For $R = 1000$, the cubes have a number of spectral channels N_λ of 386 and 357 for the BB_J and BB_H filters. For the spatial resolution, we set the image plate scale to 16 mas/pixel to be at Nyquist sampling at 1.2 μm. Assuming 35×35 pixels in our simulations, this leads to a field of view (FoV) of 560×560 mas^2. The spectral resolution, bandwidth and FoV can further be adjusted to produce the corresponding data cubes and explore the expected science return for different MedRes configurations.

For the data processing and analysis of data cubes with coronagraph, we wish to probe astrophysical scenes combining star and planet with different planet separation, position angle, flux, and spectra for planetary companion detection and spectral characterization. In this first round of simulations, we model the signals of given star and planet separately using light propagation from an on-axis point source respectively with and without coronagraph. The planet signal is then modulated with the coronagraph throughput as a function of separation and shifted from optical axis at a given separation. We then weight the signals with their spectrum and sum the star and planet contribution afterwards to produce data cubes with our astrophysical scene.

Our generated data output have been produced with two distinct Fourier-based codes using python, the first one based on a package from previous coronagraph design studies[20] and the second one based on HCIpy,[21] both leading to consistent results.

4.1.2 Additional noise sources

To mimic our astrophysical scene, we use the PHOENIX stellar models and put the parameters (effective temperature Teff, radius and surface gravity log(g)) used for the different systems in Table 2.

In our simulations, we inject the spectrum of a fake planet in all the individual spectral cubes from the synthetic sequence of observation. For the telescope and instrument, we assume a total throughput of 10%. On top of the speckles noise from the AO residuals that were already included in the spectral cubes, we consider both photon noise and a readout noise of 1e^- RMS.

4.1.3 Molecular mapping implementation

Before applying molecular mapping, we collapsed the individual spectral cubes in which the fake planet has been injected into one to obtain a spectral cube of 1-hour of observation (see Fig. 9 left frame). As the speckles modulate the spectra present in the cube, we remove most of the stellar speckles by performing the following operation on each spatial pixel (spaxel)

$$\text{spaxel}\,(i,j) \quad \rightarrow \quad \text{spaxel}\,(i,j) \;-\; \text{ref\_spectrum\_star} \;\times\; \texttt{savitzky-golay}\left(\frac{\text{spaxel}\,(i,j)}{\text{ref\_spectrum\_star}}\right), \qquad (1)$$

in which we use the reference spectrum of the star built as the average spectrum from the 1% brightest spaxels, and the ratio between the spaxel (i,j) and the reference spectrum of the star smoothed with a Savitzky–Golay filter (see Fig. 9 middle frame).

We then apply molecular mapping by performing a cross-correlation between the observed planetary signature and a template spectrum representing the expected planetary signature shifted at different radial velocities to measure their similarity. This operation is performed independently for each spaxel to produce a cross-correlated map for each radial velocity shift (see Figs. 9 right frame and 10). Finally, we estimate the signal-to-noise ratio for each spatial pixel and radial velocity shift, either from the cross-correlated maps by considering the velocity dimension,[22] or from temporal, spatial or spectral dimension.[23] In the following results, we use the method from Landman et al. (in prep) to estimate the signal-to-noise ratio. This is based on the analytical signal-to-noise (S/N) ratio of a matched filter under i.i.d. noise, which is given by:[23]

$$S/N = \frac{\sum_i^N s_i t_i / \sigma_i^2}{\sqrt{\sum_i t_i^2 / \sigma_i^2}}, \tag{2}$$

where s_i are the noisy residuals, t_i the cross-correlation template and σ_i the uncertainties. Since all noise sources are exactly known in the simulations, we can directly use Eq. (2) to estimate the detection S/N. For this matched filter we consider both the spectral domain (planet spectrum) as well as the spatial domain (shape of the point spread function [PSF]), which is assumed to be a Gaussian with appropriate full width at half maximum (FWHM) for the given wavelength. In future work, we will provide a comparison of the different metrics used in the literature to estimate the signal-to-noise ratio.

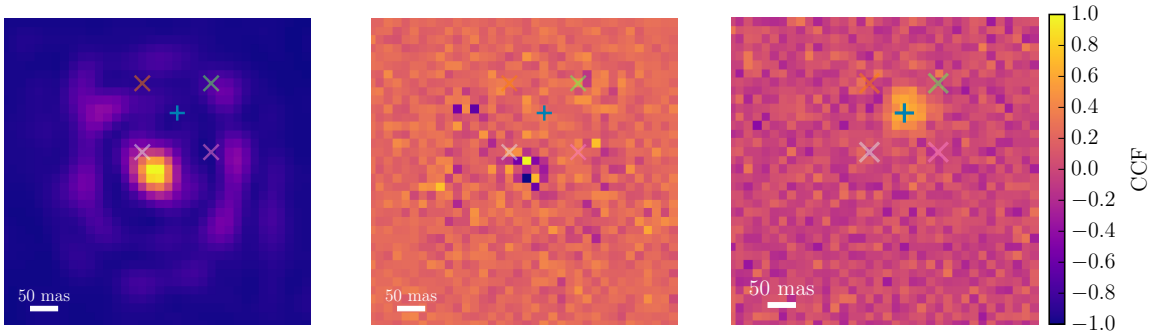

Figure 9. On the left, example of a coronagraphic image at a given wavelength of an observed star from the simulated spectral cube with the fake planet injected here at a contrast of $5 \cdot 10^{-5}$. The AO residuals, photon and read-out noise are included in this image. In the middle, the same image after subtraction the stellar halo. On the right, representation of the cross-correlation map at a radial velocity shift of 0 km/s. The markers represent the location of the injected fake planet ('plus' in blue) and four additional locations indicating the noise level ('crosses' in different colors).

4.2 Early results

Using the generated spectral cubes and data analysis described above, we can estimate the expected performance of MedRes. We do this by simulating mock observations of three archetypical directly imaged planets using the instrumental specifications from Fig. 2. The assumed parameters for these systems are specified in Table 2. The mock observations assume a total exposure time of 1 hour, divided into 60 exposures. We iteratively inject planets with different contrasts in the resulting data cubes and try to recover them using molecule mapping. This is averaged for ten different position angles and the planet is considered detected if we achieve a signal-to-noise ratio > 5. This process is repeated for different angular separations, instrument concepts and observing settings, and the resulting limiting contrasts are shown in Fig. 11. These show that deep contrasts $< 10^{-5}$ can be achieved close to the inner working angle of the coronagraph for each of these systems. The deepest contrasts can be reached for a 51 Eri b-like planet, which has relatively more molecular features due to its lower temperature.

ACKNOWLEDGMENTS

This work has been supported by the PRIN-INAF 2019 "Planetary systems at young ages (PLATEA)" and ASI-INAF agreement n.2018-16-HH.0.

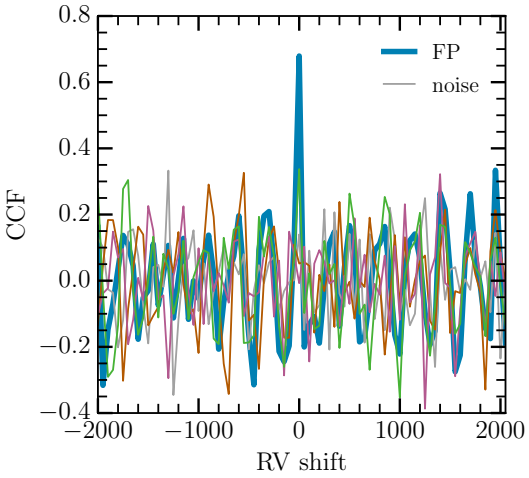

Figure 10. Cross-correlation function at the location of the injected fake planet (FP) and at four additional locations to indicate the noise level. These locations are shown in Fig. 9 via the markers 'plus' in blue for the fake planet, and 'crosses' in different colors for the noise.

Table 2. Assumed parameters of the planetary systems used to estimate the performance of MedRes. For both the star and the planet we use a surface gravity log(g) of 4.0.

Planet	R_*	T_*	Distance	R_p	T_p
β Pic b	1.8 $R_\odot$	8100 K	19.44 pc	1.36 $R_{\rm jup}$	1700 K
HR8799 e	1.34 $R_\odot$	7400 K	40.88 pc	1.12 $R_{\rm jup}$	1200 K
51 Eri b	1.45 $R_\odot$	7200 K	29.4 pc	1.1 $R_{\rm jup}$	700 K

REFERENCES

[1] Beuzit, J. L., Vigan, A., Mouillet, D., Dohlen, K., Gratton, R., Boccaletti, A., Sauvage, J. F., Schmid, H. M., Langlois, M., Petit, C., Baruffolo, A., Feldt, M., Milli, J., Wahhaj, Z., Abe, L., Anselmi, U., Antichi, J., Barette, R., Baudrand, J., Baudoz, P., Bazzon, A., Bernardi, P., Blanchard, P., Brast, R., Bruno, P., Buey, T., Carbillet, M., Carle, M., Cascone, E., Chapron, F., Charton, J., Chauvin, G., Claudi, R., Costille, A., De Caprio, V., de Boer, J., Delboulbé, A., Desidera, S., Dominik, C., Downing, M., Dupuis, O., Fabron, C., Fantinel, D., Farisato, G., Feautrier, P., Fedrigo, E., Fusco, T., Gigan, P., Ginski, C., Girard, J., Giro, E., Gisler, D., Gluck, L., Gry, C., Henning, T., Hubin, N., Hugot, E., Incorvaia, S., Jaquet, M., Kasper, M., Lagadec, E., Lagrange, A. M., Le Coroller, H., Le Mignant, D., Le Ruyet, B., Lessio, G., Lizon, J. L., Llored, M., Lundin, L., Madec, F., Magnard, Y., Marteaud, M., Martinez, P., Maurel, D., Ménard, F., Mesa, D., Möller-Nilsson, O., Moulin, T., Moutou, C., Origné, A., Parisot, J., Pavlov, A., Perret, D., Pragt, J., Puget, P., Rabou, P., Ramos, J., Reess, J. M., Rigal, F., Rochat, S., Roelfsema, R., Rousset, G., Roux, A., Saisse, M., Salasnich, B., Santambrogio, E., Scuderi, S., Segransan, D., Sevin, A., Siebenmorgen, R., Soenke, C., Stadler, E., Suarez, M., Tiphène, D., Turatto, M., Udry, S., Vakili, F., Waters, L. B. F. M., Weber, L., Wildi, F., Zins, G., and Zurlo, A., "SPHERE: the exoplanet imager for the Very Large Telescope," *Astron. & Astrophys.* **631**, A155 (Nov. 2019).

[2] et Al., A. B., "Upgrading the high contrast imaging facility sphere: science drivers and instrument choices," in [Ground-based and Airborne Instrumentation for Astronomy IX], Proc. SPIE **12184** (2022).

[3] Claudi, R. U., Turatto, M., Gratton, R. G., Antichi, J., Bonavita, M., Bruno, P., Cascone, E., De Caprio, V., Desidera, S., Giro, E., Mesa, D., Scuderi, S., Dohlen, K., Beuzit, J. L., and Puget, P., "SPHERE IFS: the spectro differential imager of the VLT for exoplanets search," in [Ground-based and Airborne Instrumentation for Astronomy II], McLean, I. S. and Casali, M. M., eds., Society of Photo-Optical Instrumentation Engineers (SPIE) Conference Series **7014**, 70143E (July 2008).

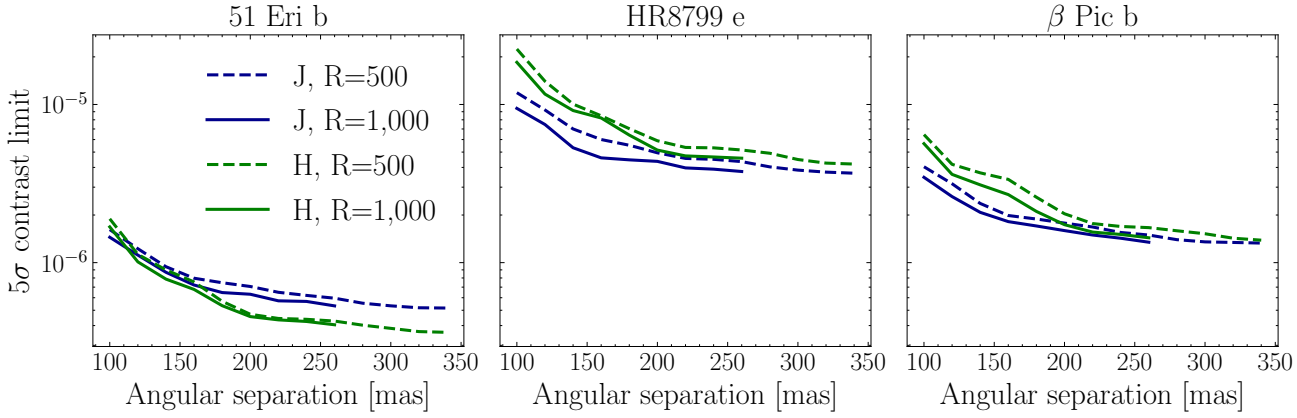

Figure 11. Estimated 5σ contrast limits for the lenslet designs of MedRes in the J and H band and for the two instrument configurations. The only data analysis method considered here is molecular mapping.

[4] Marois, C., Lafrenière, D., Doyon, R., Macintosh, B., and Nadeau, D., "Angular Differential Imaging: A Powerful High-Contrast Imaging Technique," *Astrophys. J.* **641**, 556–564 (Apr. 2006).

[5] Thatte, N., Abuter, R., Tecza, M., Nielsen, E. L., Clarke, F. J., and Close, L. M., "Very high contrast integral field spectroscopy of AB Doradus C: 9-mag contrast at 0.2arcsec without a coronagraph using spectral deconvolution†," *Monthly Not. Roy. Astron. Soc.* **378**, 1229–1236 (July 2007).

[6] Mesa, D., Gratton, R., Zurlo, A., Vigan, A., Claudi, R. U., Alberi, M., Antichi, J., Baruffolo, A., Beuzit, J. L., Boccaletti, A., Bonnefoy, M., Costille, A., Desidera, S., Dohlen, K., Fantinel, D., Feldt, M., Fusco, T., Giro, E., Henning, T., Kasper, M., Langlois, M., Maire, A. L., Martinez, P., Moeller-Nilsson, O., Mouillet, D., Moutou, C., Pavlov, A., Puget, P., Salasnich, B., Sauvage, J. F., Sissa, E., Turatto, M., Udry, S., Vakili, F., Waters, R., and Wildi, F., "Performance of the VLT Planet Finder SPHERE. II. Data analysis and results for IFS in laboratory," *Astron. & Astrophys.* **576**, A121 (Apr. 2015).

[7] Hoeijmakers, H. J., Schwarz, H., Snellen, I. A. G., de Kok, R. J., Bonnefoy, M., Chauvin, G., Lagrange, A. M., and Girard, J. H., "Medium-resolution integral-field spectroscopy for high-contrast exoplanet imaging. Molecule maps of the β Pictoris system with SINFONI," *Astron. & Astrophys.* **617**, A144 (Oct. 2018).

[8] C., G., R., V. F. G., A., B., F., C., E., G., A., S., F., F., G., C., M., L., and J., M., "Saxo+ upgrade: system choices and numerical simulations," in [Adaptive Optics Systems VIII], Proc. SPIE **12185** (2022).

[9] Stadler, E., Diolaiti, E., Schreiber, L., Cortecchia, F., Lombini, M., Rosa, A. D., Malaguti, G., Maurel, D., Morgante, G., Rabou, P., Rochat, S., Schiavone, F., Terenzi, L., Loupias, M., Magnard, Y., Vidal, F., Cantalloube, F., Gendron, E., R. Gratton, J. M., Mouillet, D., Chauvin, G., Wildi, F., Beuzit, J.-L., and Boccaletti, A., "Saxo+, a second-stage adaptive optics for sphere on vlt: optical and mechanical design concept," in [Adaptive Optics Systems VIII], Proc. SPIE **12185** (2022).

[10] Vigan, A., Otten, G. P. P. L., Muslimov, E., Dohlen, K., Philipps, M. W., Seemann, U., Beuzit, J. L., Dorn, R., Kasper, M., Mouillet, D., Baraffe, I., and Reiners, A., "Bringing high-spectral resolution to VLT/SPHERE with a fiber coupling to VLT/CRIRES+," in [Ground-based and Airborne Instrumentation for Astronomy VII], Evans, C. J., Simard, L., and Takami, H., eds., Society of Photo-Optical Instrumentation Engineers (SPIE) Conference Series **10702**, 1070236 (July 2018).

[11] Finger, G., Baker, I., Alvarez, D., Eisenhauer, F., Hechenblaikner, G., Ives, D., Mehrgan, L., Meyer, M., Stegmeier, J., and Weller, H. J., "On-sky performance verification of near infrared eAPD technology for wavefront sensing at ground based telescopes, demonstration of e-APD pixel performance to improve the sensitivity of large science focal planes and possibility to use this technology in space," in [International Conference on Space Optics — ICSO 2018], Society of Photo-Optical Instrumentation Engineers (SPIE) Conference Series **11180**, 111806L (July 2019).

[12] Haffert, S. Y., Harris, R. J., Zanutta, A., Pike, F. A., Bianco, A., Redaelli, E., BenoÃ®t, A., MacLachlan, D. G., Ross, C. A., Gris-Sánchez, I., Trappen, M. D., Xu, Y., Blaicher, M., Maier, P., Riva, G., Sinquin, B., Kulcsár, C., Bharmal, N. A., Gendron, E., Staykov, L., Morris, T. J., Barboza, S., Muench, N., Bardou,

L., Prengère, L., Raynaud, H.-F., Hottinger, P., Anagnos, T., Osborn, J., Koos, C., Thomson, R. R., Birks, T. A., Snellen, I. A. G., and Keller, C. U., "Diffraction-limited integral-field spectroscopy for extreme adaptive optics systems with the multicore fiber-fed integral-field unit," Journal of Astronomical Telescopes, Instruments, and Systems **6**, 045007 (Oct. 2020).

[13] Petrov, R. G., Malbet, F., Weigelt, G., Antonelli, P., Beckmann, U., Bresson, Y., Chelli, A., Dugué, M., Duvert, G., Gennari, S., Glück, L., Kern, P., Lagarde, S., Le Coarer, E., Lisi, F., Millour, F., Perraut, K., Puget, P., Rantakyrö, F., Robbe-Dubois, S., Roussel, A., Salinari, P., Tatulli, E., Zins, G., Accardo, M., Acke, B., Agabi, K., Altariba, E., Arezki, B., Aristidi, E., Baffa, C., Behrend, J., Blöcker, T., Bonhomme, S., Busoni, S., Cassaing, F., Clausse, J. M., Colin, J., Connot, C., Delboulbé, A., Domiciano de Souza, A., Driebe, T., Feautrier, P., Ferruzzi, D., Forveille, T., Fossat, E., Foy, R., Fraix-Burnet, D., Gallardo, A., Giani, E., Gil, C., Glentzlin, A., Heiden, M., Heininger, M., Hernandez Utrera, O., Hofmann, K. H., Kamm, D., Kiekebusch, M., Kraus, S., Le Contel, D., Le Contel, J. M., Lesourd, T., Lopez, B., Lopez, M., Magnard, Y., Marconi, A., Mars, G., Martinot-Lagarde, G., Mathias, P., Mège, P., Monin, J. L., Mouillet, D., Mourard, D., Nussbaum, E., Ohnaka, K., Pacheco, J., Perrier, C., Rabbia, Y., Rebattu, S., Reynaud, F., Richichi, A., Robini, A., Sacchettini, M., Schertl, D., Schöller, M., Solscheid, W., Spang, A., Stee, P., Stefanini, P., Tallon, M., Tallon-Bosc, I., Tasso, D., Testi, L., Vakili, F., von der Lühe, O., Valtier, J. C., Vannier, M., and Ventura, N., "AMBER, the near-infrared spectro-interferometric three-telescope VLTI instrument," *Astron. & Astrophys.* **464**, 1–12 (Mar. 2007).

[14] Antichi, J., Dohlen, K., Gratton, R. G., Mesa, D., Claudi, R. U., Giro, E., Boccaletti, A., Mouillet, D., Puget, P., and Beuzit, J.-L., "BIGRE: A Low Cross-Talk Integral Field Unit Tailored for Extrasolar Planets Imaging Spectroscopy," Astrophysical Journal **695**, 1042–1057 (Apr. 2009).

[15] Vigan, A., N'Diaye, M., Dohlen, K., Sauvage, J. F., Milli, J., Zins, G., Petit, C., Wahhaj, Z., Cantalloube, F., Caillat, A., Costille, A., Le Merrer, J., Carlotti, A., Beuzit, J. L., and Mouillet, D., "Calibration of quasi-static aberrations in exoplanet direct-imaging instruments with a Zernike phase-mask sensor. III. On-sky validation in VLT/SPHERE," *Astron. & Astrophys.* **629**, A11 (Sept. 2019).

[16] Fusco, T., Sauvage, J. F., Mouillet, D., Costille, A., Petit, C., Beuzit, J. L., Dohlen, K., Milli, J., Girard, J., Kasper, M., Vigan, A., Suarez, M., Soenke, C., Downing, M., N'Diaye, M., Baudoz, P., Sevin, A., Baruffolo, A., Schmid, H. M., Salasnich, B., Hugot, E., and Hubin, N., "SAXO, the SPHERE extreme AO system: on-sky final performance and future improvements," in [Adaptive Optics Systems V], Marchetti, E., Close, L. M., and Véran, J.-P., eds., Society of Photo-Optical Instrumentation Engineers (SPIE) Conference Series **9909**, 99090U (July 2016).

[17] Cantalloube, F., Dohlen, K., Milli, J., Brandner, W., and Vigan, A., "Peering through SPHERE Images: A Glance at Contrast Limitations," The Messenger **176**, 25–31 (June 2019).

[18] Soummer, R., "Apodized Pupil Lyot Coronagraphs for Arbitrary Telescope Apertures," Astrophysical Journal Letters **618**, L161–L164 (Jan. 2005).

[19] Martinez, P., Dorrer, C., Aller Carpentier, E., Kasper, M., Boccaletti, A., Dohlen, K., and Yaitskova, N., "Design, analysis, and testing of a microdot apodizer for the Apodized Pupil Lyot Coronagraph," *Astron. & Astrophys.* **495**, 363–370 (Feb. 2009).

[20] N'Diaye, M., Soummer, R., Pueyo, L., Carlotti, A., Stark, C. C., and Perrin, M. D., "Apodized Pupil Lyot Coronagraphs for Arbitrary Apertures. V. Hybrid Shaped Pupil Designs for Imaging Earth-like planets with Future Space Observatories," *Astrophys. J.* **818**, 163 (Feb. 2016).

[21] Por, E. H., Haffert, S. Y., Radhakrishnan, V. M., Doelman, D. S., van Kooten, M., and Bos, S. P., "High Contrast Imaging for Python (HCIPy): an open-source adaptive optics and coronagraph simulator," in [Adaptive Optics Systems VI], Close, L. M., Schreiber, L., and Schmidt, D., eds., Society of Photo-Optical Instrumentation Engineers (SPIE) Conference Series **10703**, 1070342 (July 2018).

[22] Cugno, G., Patapis, P., Stolker, T., Quanz, S. P., Boehle, A., Hoeijmakers, H. J., Marleau, G.-D., Molliè re, P., Nasedkin, E., and Snellen, I. A. G., "Molecular mapping of the PDS70 system," Astronomy & Astrophysics **653**, A12 (aug 2021).

[23] Houllé, M., Vigan, A., Carlotti, A., Choquet, É., Cantalloube, F., Phillips, M. W., Sauvage, J. F., Schwartz, N., Otten, G. P. P. L., Baraffe, I., Emsenhuber, A., and Mordasini, C., "Direct imaging and spectroscopy of exoplanets with the ELT/HARMONI high-contrast module," Astronomy & Astrophysics **652**, A67 (Aug. 2021).